

000
001
002
003
004
005
006
007
008
009
010
011
012
013
014
015
016
017
018
019
020
021
022
023
024
025
026
027
028
029
030
031
032
033
034
035
036
037
038
039
040
041
042
043
044

Supplementary Material to “A Trilateral Weighted Sparse Coding Scheme for for Real-World Image Denoising”

005
006
007
008
009
010
011
012
013
014
015
016
017
018
019
020
021
022
023
024
025
026
027
028
029
030
031
032
033
034
035
036
037
038
039
040
041
042
043
044

Jun Xu¹, Lei Zhang^{1*}, David Zhang^{1,2}

¹The Hong Kong Polytechnic University, Hong Kong SAR, China

²School of Science and Engineering, The Chinese University of Hong Kong
(Shenzhen), Shenzhen, China

{csjunxu, cs1zhang}@comp.polyu.edu.hk

In this supplementary file, we provide:

1. The proof of Theorem 1 in the main paper;
2. Denoising results on the 20 gray level images;
3. More denoising results on the real noisy images of dataset [1];
4. More denoising results on the real noisy images of dataset [2];
5. More denoising results on the real noisy images of dataset [3].

1 Proof of Theorem 1

Theorem 1. Assume that $\mathbf{A} \in \mathbb{R}^{3p^2 \times 3p^2}$, $\mathbf{B} \in \mathbb{R}^{M \times M}$ are both symmetric and positive semi-definite matrices. If at least one of \mathbf{A}, \mathbf{B} is positive definite, the Sylvester equation $\mathbf{AC} + \mathbf{CB} = \mathbf{E}$ has a unique solution for $\mathbf{C} \in \mathbb{R}^{3p^2 \times M}$.

Proof. Since \mathbf{A}, \mathbf{B} are symmetric matrices, they can be diagonalized as $\mathbf{A} = \mathbf{U}_A \boldsymbol{\Sigma}_A \mathbf{U}_A^\top$, $\mathbf{B} = \mathbf{U}_B \boldsymbol{\Sigma}_B \mathbf{U}_B^\top$, where $\boldsymbol{\Sigma}_A = \text{diag}(\lambda_A^1, \dots, \lambda_A^{3p^2})$ and $\boldsymbol{\Sigma}_B = \text{diag}(\lambda_B^1, \dots, \lambda_B^M)$ are diagonal matrices. Since \mathbf{A}, \mathbf{B} are positive semi-definite matrices, their corresponding eigenvalues are non-negative, i.e., $\lambda_A^i \geq 0$ for $\forall i = 1, \dots, 3p^2$ and $\lambda_B^j \geq 0$ for $\forall j = 1, \dots, M$. If at least one of the matrices \mathbf{A}, \mathbf{B} is positive definite, then $\lambda_A^i + \lambda_B^j > 0$ holds true for $\forall i, j$ and $\sigma(\mathbf{A}) \cap \sigma(-\mathbf{B}) = \emptyset$. Therefore, the Sylvester equation $\mathbf{AC} + \mathbf{CB} = \mathbf{E}$ has a unique solution.

2 Denoising results on the 20 gray level images

In this section, we compare the competing methods on the 20 widely used images (listed in Fig. 1) in Figures 5–9. The compared methods include BM3D-SAPCA [4], LSSC [5], NCSR [6], WNNM [7], TNRD [8], DnCNN [9], and the baseline method WSC described in the main paper.

3 More denoising results on the real noisy images of dataset [1]

In this section, we give more visual comparisons of the competing methods on the dataset [1]. Fig. 2 shows 10 sample images of this dataset. The real noisy images

* This project is supported by Hong Kong RGC GRF project (PolyU 152124/15E).



Fig. 1. The 20 widely used gray level test images.

in dataset [1] have no “ground truth” images and hence we only compare the visual quality of the denoised images by different methods. The compared methods include CBM3D [10], TNRD [8], DnCNN [9], NI [11], NC [12], MCWNNM [13], and the baseline WSC method. As shown in Figures 10–12, our proposed method produces perceptually more pleasing results than the competing methods.



Fig. 2. The 10 sample images from dataset [1].

4 More denoising results on the real noisy images of dataset [2]

In this section, we give more visual comparisons of the competing methods on the 15 cropped real noisy images (listed in Fig. 3) used in [2]. In this dataset, each scene was shot 500 times under the same camera and camera setting. The mean image of the 500 shots is roughly taken as the “ground truth”, with which the PSNR and SSIM [14] can be computed. The compared methods include CBM3D [10], TNRD [8], DnCNN [9], NI [11], NC [12], CC [2], and MCWNNM [13]. As shown in Figures 13–15, our proposed TWSC method produces perceptually more pleasing results than the the competing methods.



Fig. 3. The 15 cropped real noisy images from dataset [2].

5 More denoising results on the real noisy images of dataset [3]

In this section, we give more visual comparisons of the competing methods on the 10 cropped real noisy images (listed in Fig. 4) used in [3]. In this dataset, each scene was shot twice, one at a high ISO value and the other at a low ISO value. The image captured at low ISO value (usually 100 or 125) is roughly taken

as the “ground truth”, with which the PSNR and SSIM [14] can be computed. The compared methods include CBM3D [10], TNRD [8], DnCNN [9], NI [11], NC [12], MCWNNM [13], and the baseline WSC method. As shown in Figures 16–18, our proposed TWSC method produces perceptually more pleasing results than the competing methods.



Fig. 4. The 10 cropped real noisy images from dataset [3].

References

- Lebrun, M., Colom, M., Morel, J.M.: The noise clinic: a blind image denoising algorithm. <http://www.ipol.im/pub/art/2015/125/> Accessed 01 28, 2015. 1, 2, 9, 10, 11
- Nam, S., Hwang, Y., Matsushita, Y., Kim, S.J.: A holistic approach to cross-channel image noise modeling and its application to image denoising. In: CVPR (2016) 1683–1691 1, 2, 12, 13, 14
- Plötz, T., Roth, S.: Benchmarking denoising algorithms with real photographs. In: CVPR. (2017) 1, 2, 3, 15, 16, 17
- Dabov, K., Foi, A., Katkovnik, V., Egiazarian, K.: Bm3d image denoising with shape-adaptive principal component analysis. In: SPARS. (2009) 1
- Mairal, J., Bach, F., Ponce, J., Sapiro, G., Zisserman, A.: Non-local sparse models for image restoration. In: ICCV. (2009) 2272–2279 1
- Dong, W., Zhang, L., Shi, G., Li, X.: Nonlocally centralized sparse representation for image restoration. IEEE Transactions on Image Processing **22**(4) (2013) 1620–1630 1
- Gu, S., Zhang, L., Zuo, W., Feng, X.: Weighted nuclear norm minimization with application to image denoising. In: CVPR, IEEE (2014) 2862–2869 1
- Chen, Y., Yu, W., Pock, T.: On learning optimized reaction diffusion processes for effective image restoration. In: CVPR (2015) 5261–5269 1, 2, 3
- Zhang, K., Zuo, W., Chen, Y., Meng, D., Zhang, L.: Beyond a Gaussian denoiser: Residual learning of deep cnn for image denoising. IEEE Transactions on Image Processing (2017) 1, 2, 3
- Dabov, K., Foi, A., Katkovnik, V., Egiazarian, K.: Color image denoising via sparse 3D collaborative filtering with grouping constraint in luminance-chrominance space. In: ICIP, IEEE (2007) 313–316 2, 3
- ABSoft, N.: Neat Image. <https://ni.neatvideo.com/home> 2, 3
- Lebrun, M., Colom, M., Morel, J.M.: Multiscale image blind denoising. IEEE Transactions on Image Processing **24**(10) (2015) 3149–3161 2, 3
- Xu, J., Zhang, L., Zhang, D., Feng, X.: Multi-channel weighted nuclear norm minimization for real color image denoising. In: ICCV. (2017) 2, 3
- Wang, Z., Bovik, A.C., Sheikh, H.R., Simoncelli, E.P.: Image quality assessment: from error visibility to structural similarity. IEEE Transactions on Image Processing **13**(4) (2004) 600–612 2, 3

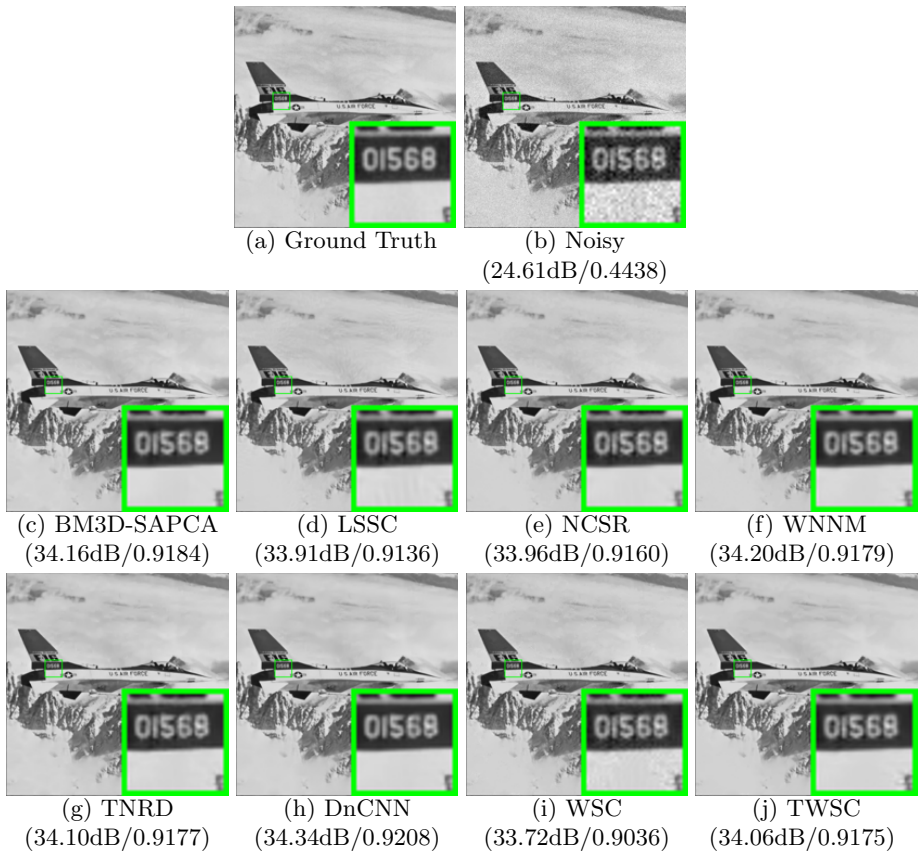


Fig. 5. Denoised images and PSNR/SSIM results of Airplane by different methods (the noise level is $\sigma = 15$).

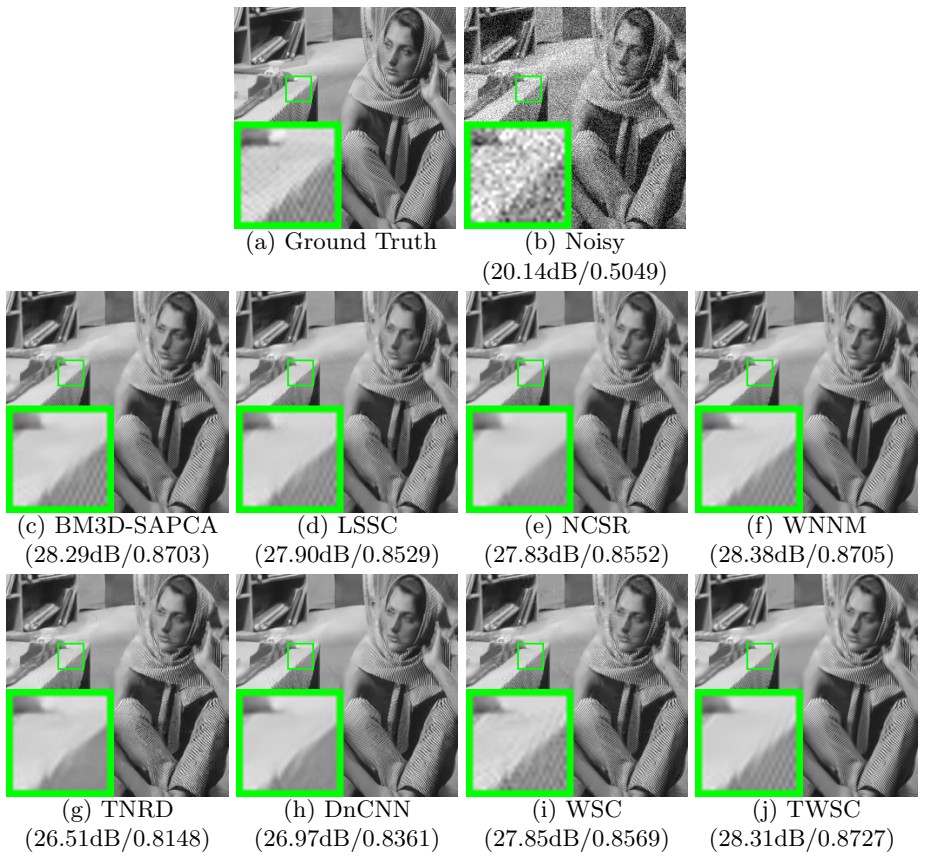


Fig. 6. Denoised images and PSNR/SSIM results of *Barbara* by different methods (the noise level is $\sigma = 25$).

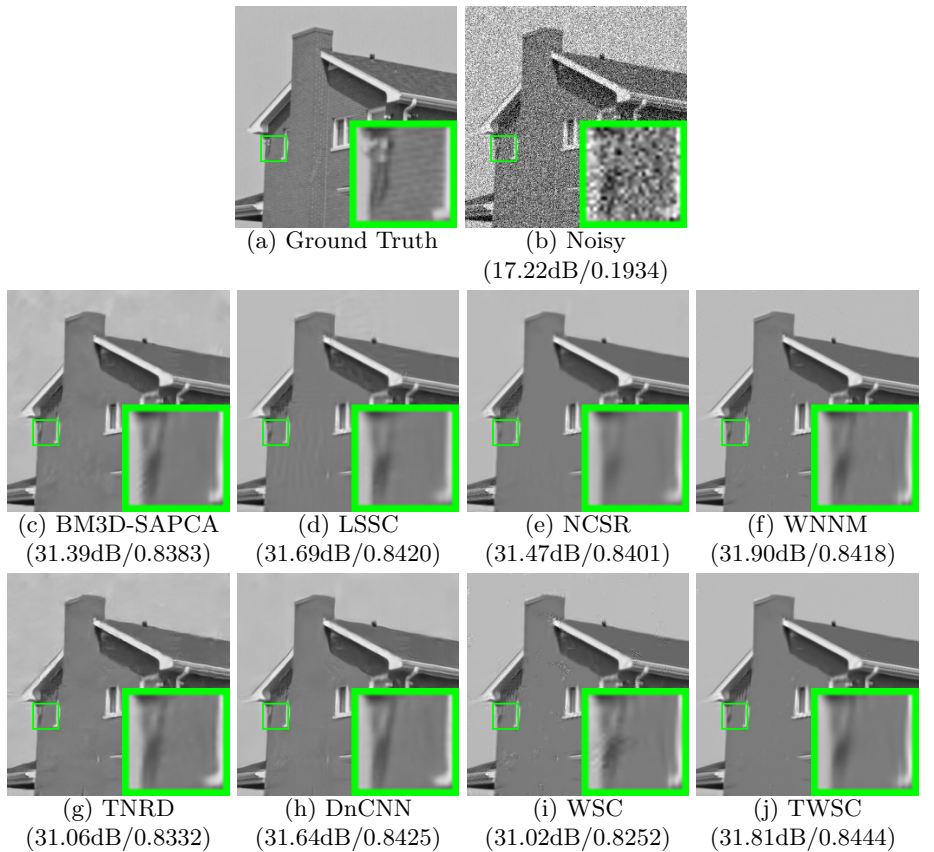


Fig. 7. Denoised images and PSNR/SSIM results of *House* by different methods (the noise level is $\sigma = 35$).

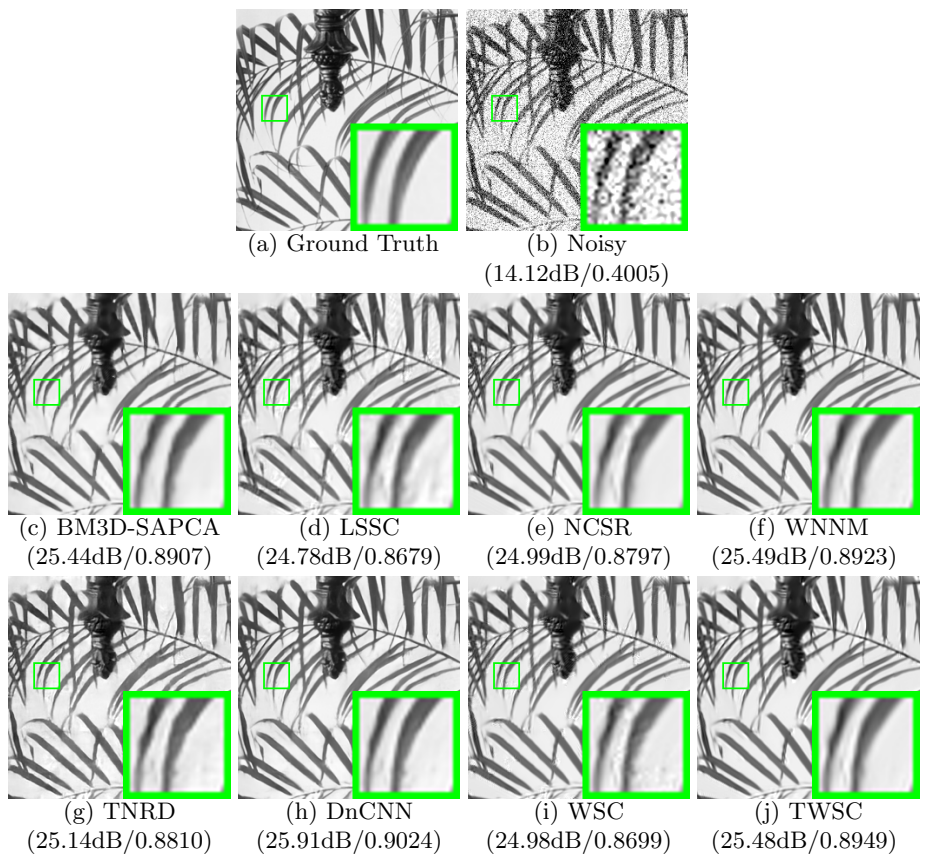


Fig. 8. Denoised images and PSNR/SSIM results of *Leaves* by different methods (the noise level is $\sigma = 50$).

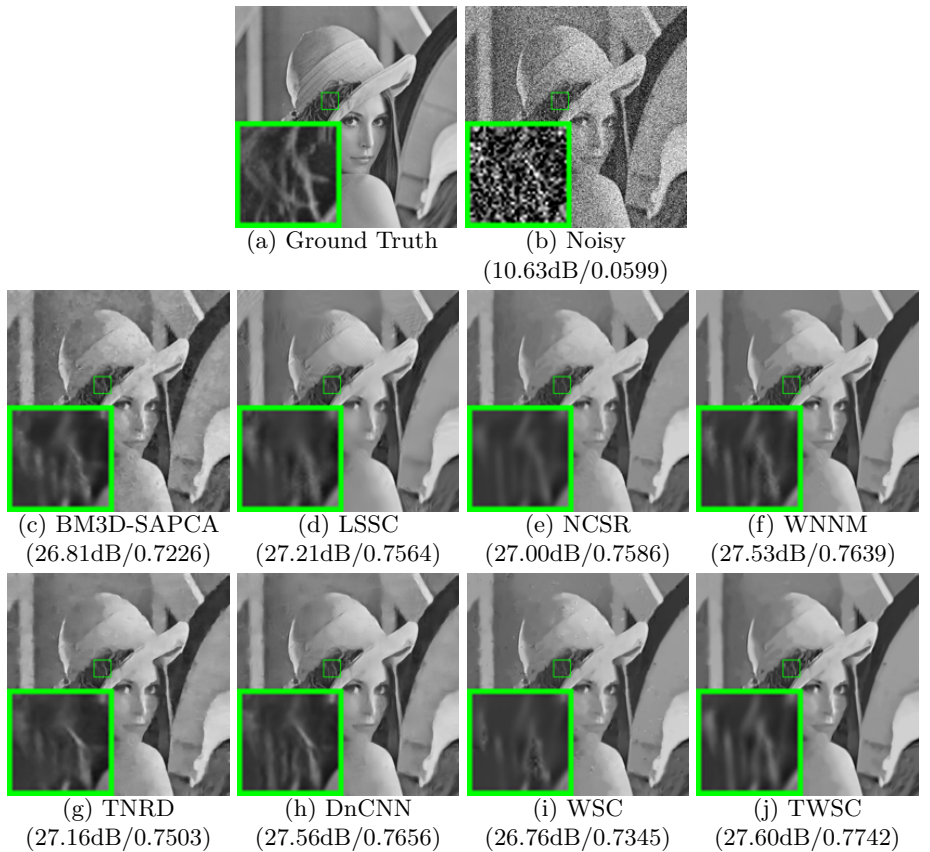


Fig. 9. Denoised images and PSNR/SSIM results of *Lena* by different methods (the noise level is $\sigma = 75$).

315
316
317
318
319
320
321
322
323
324
325
326
327
328
329
330
331
332
333
334
335
336
337
338
339
340
341
342
343
344
345
346
347
348
349
350
351
352
353
354
355
356
357
358
359

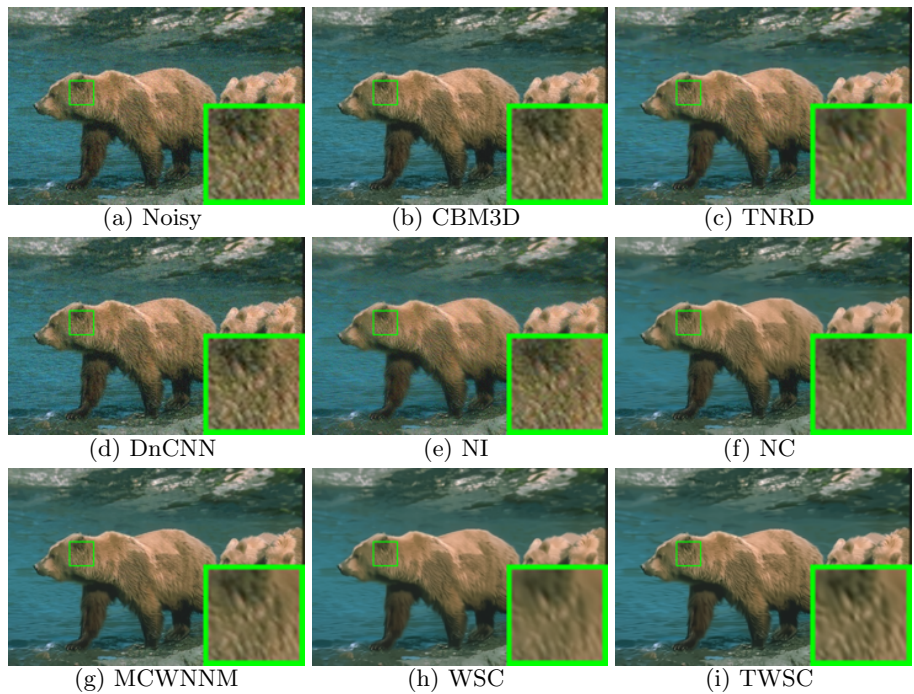


Fig. 10. Denoised images of the real noisy image Bears [1] by different methods.

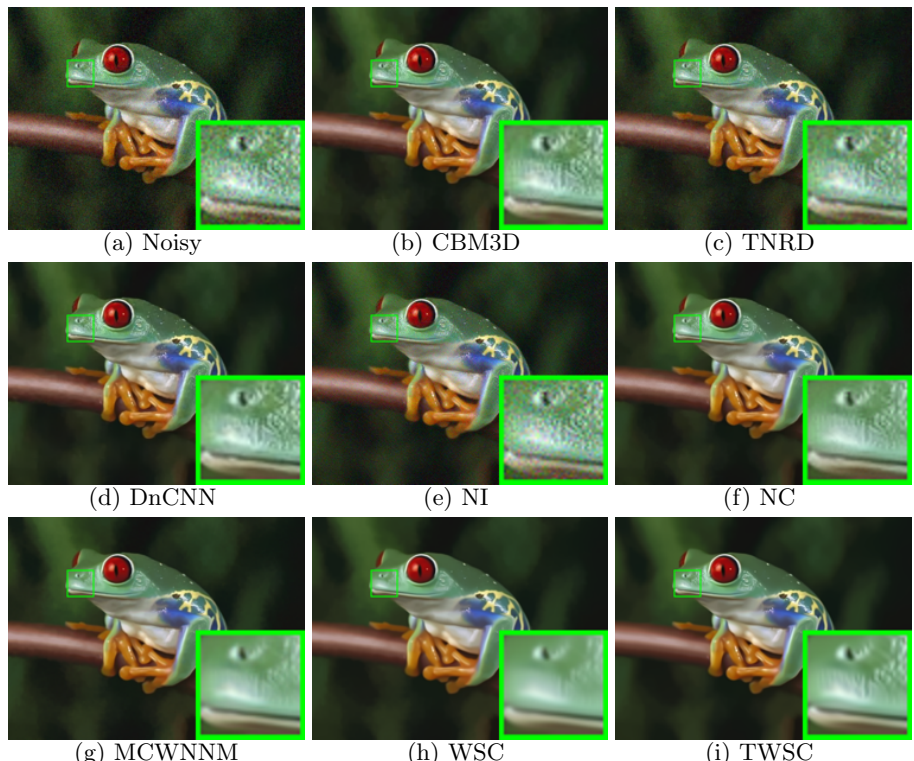


Fig. 11. Denoised images of the real noisy image *Frog* [1] by different methods.

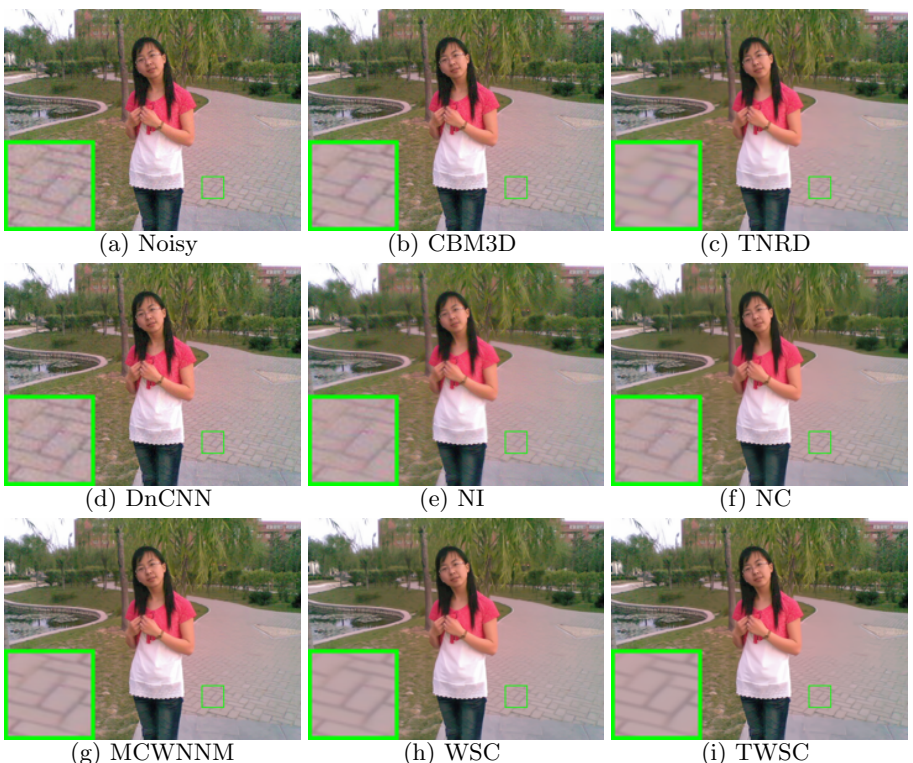


Fig. 12. Denoised images of the real noisy image *Girl* [1] by different methods.

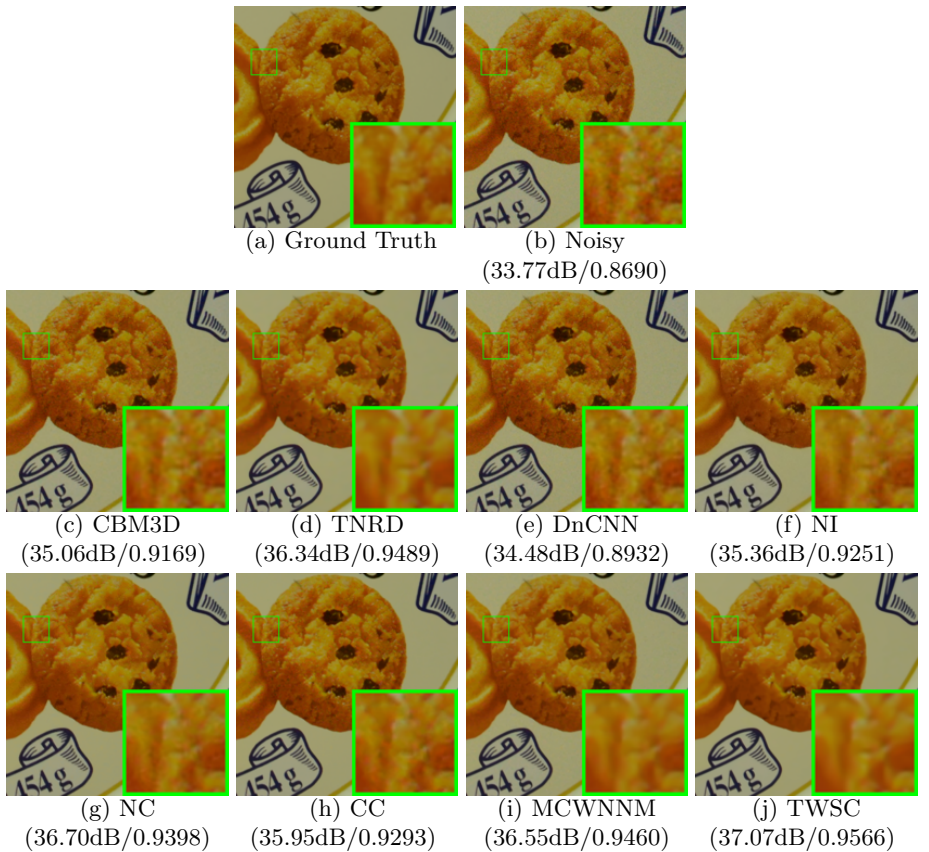


Fig. 13. Denoised images and PSNR/SSIM results of the real noisy image Nikon D600 ISO 3200 2 [2] by different methods.

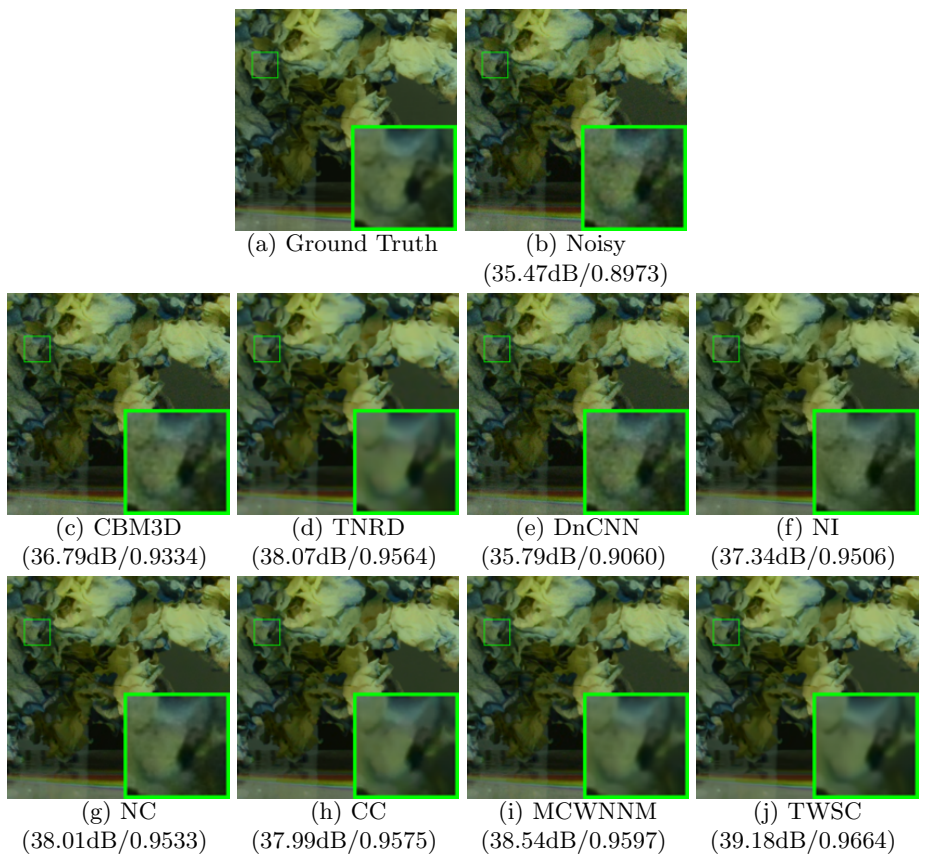


Fig. 14. Denoised images and PSNR/SSIM results of the real noisy image Nikon D800 ISO 1600 1 [2] by different methods.



Fig. 15. Denoised images and PSNR/SSIM results of the real noisy image Nikon D800 ISO 3200 1 [2] by different methods.

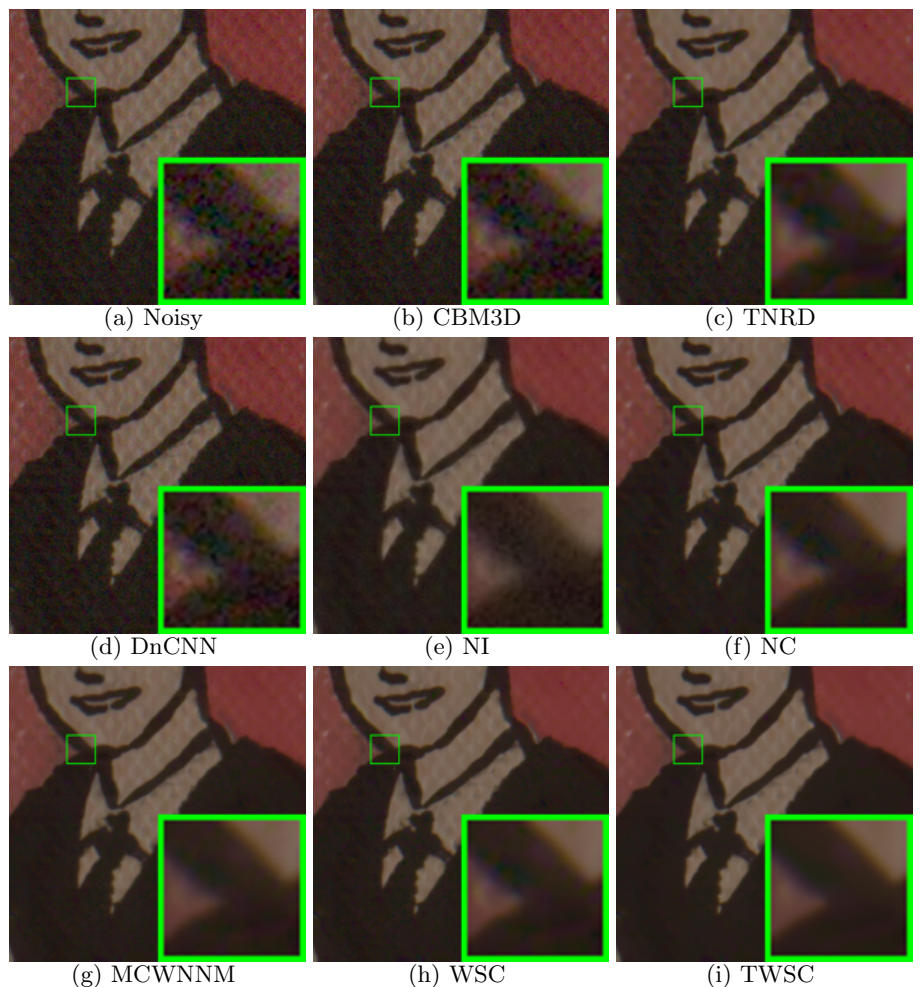


Fig. 16. Denoised images and PSNR/SSIM results of the real noisy image “0019_16” captured by Olympus E-M10 [3] by different methods.

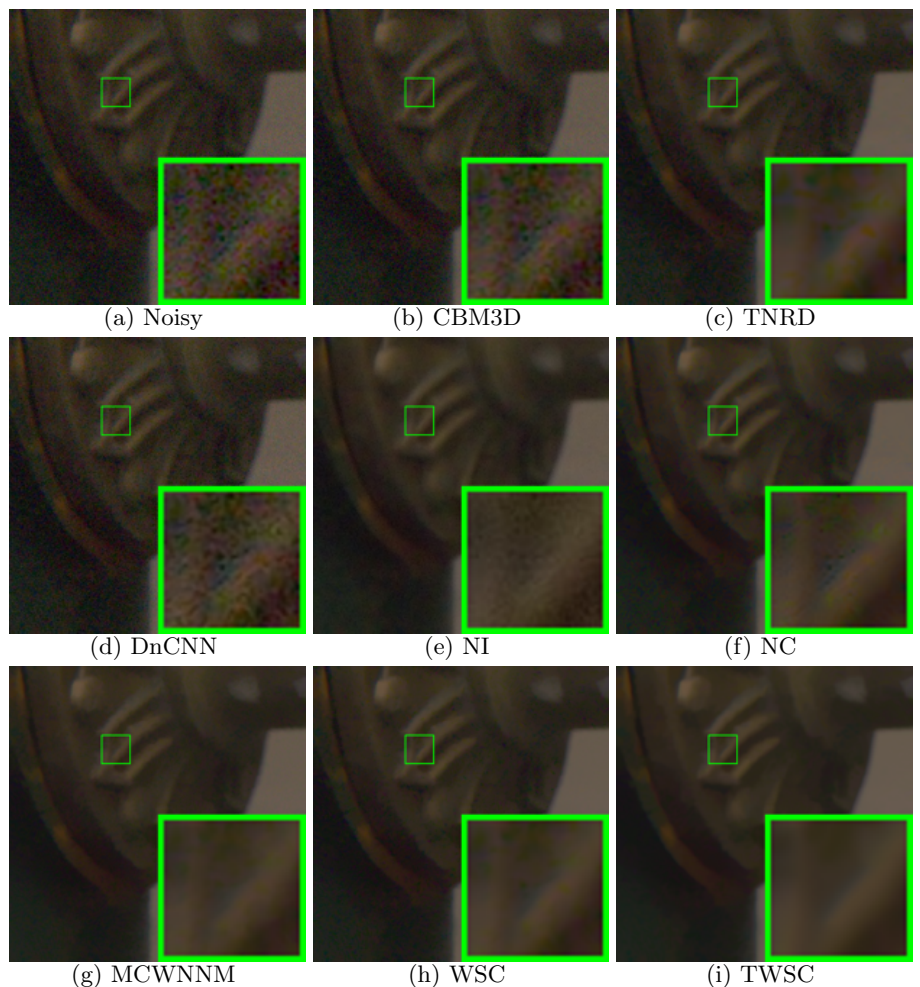


Fig. 17. Denoised images and PSNR/SSIM results of the real noisy image “0025_15” captured by Olympus E-M10 [3] by different methods.

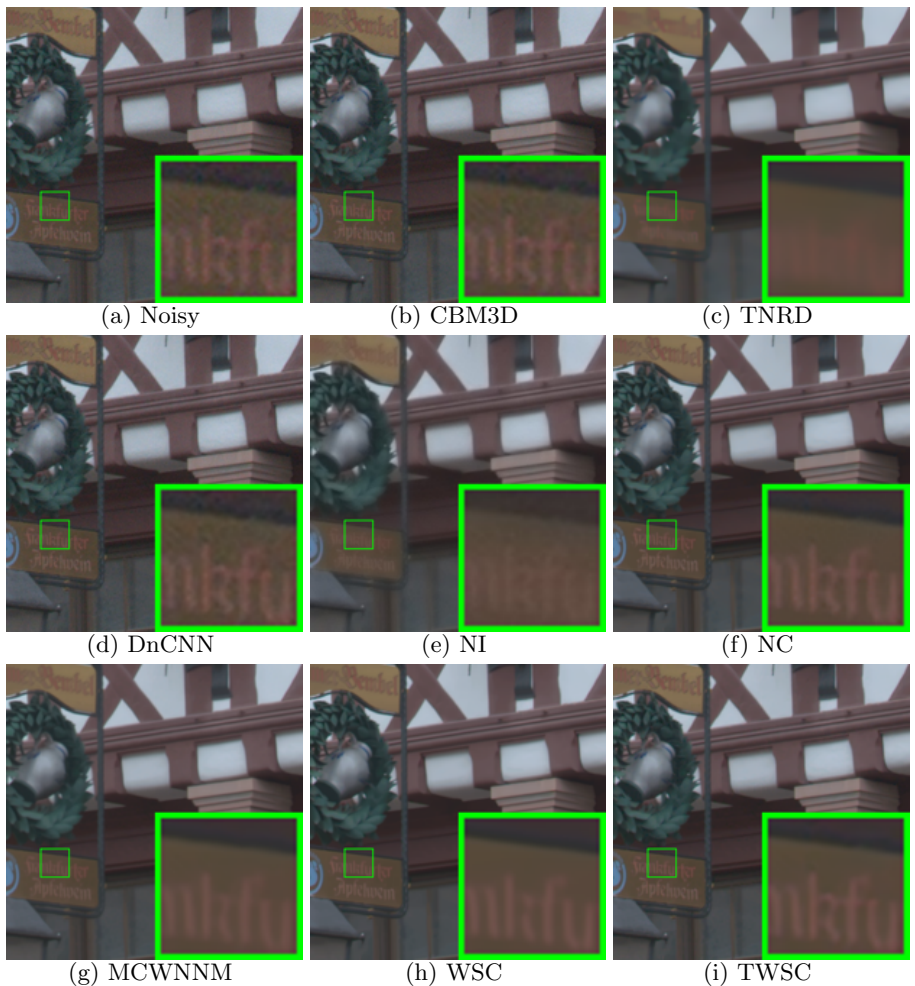


Fig. 18. Denoised images and PSNR/SSIM results of the real noisy image “0037_8” captured by Sony RX100 IV [3] by different methods.